Applied Catalysis B: Environmental 237 (2018) 401–408

Contents lists available at ScienceDirect

Applied Catalysis B: Environmental

journal homepage: www.elsevier.com/locate/apcatb

The role of surface states during photocurrent switching: Intensity modulated photocurrent spectroscopy analysis of $BiVO_4$ photoelectrodes

Manuel Antuch[a], Pierre Millet[a,*], Akihide Iwase[b], Akihiko Kudo[b]

[a] Équipe de Recherche et Innovation en Électrochimie pour l'Energie (ERIEE), Institut de Chimie Moléculaire et des Matériaux d'Orsay (ICMMO), UMR CNRS 8182, Université Paris-Sud, Université Paris-Saclay, 91405 Orsay, France

[b] Department of Applied Chemistry, Tokyo University of Science, 1-3 Kagurazaka, Shinjuku-ku, Tokyo 162-8601, Japan

ARTICLE INFO

Keywords:
IMPS
BiVO4
Photocurrent polarity switch

ABSTRACT

Intriguing photo-electrochemical characteristics of $BiVO_4$ photoelectrodes studied in pH-neutral aqueous solutions are reported herein. Indeed, we have observed photocurrent polarity switching, as put in evidence by cyclic voltammetry under chopped illumination conditions. Such unusual behavior was analyzed in detail using Intensity Modulated Photocurrent Spectroscopy (IMPS). At potentials where positive photocurrent was observed, the expected shape of IMPS was recorded, starting in quadrant (IV) at high-frequency (HF) and reaching quadrant (I) at low-frequency (LF) with two well defined semicircles. Surprisingly, in the negative photocurrent region, IMPS started in quadrant (II) at HF and ended in quadrant (III) at LF. Such highly infrequent features were interpreted here as the rotation of the IMPS spectra around the origin of the plot, due to the sign switch of the photocurrent. A model that takes into account the existence of in-band energy states at the surface of $BiVO_4$ has been used in order to account for the experimental results. It was found that (i) the surface state capacitance; (ii) the relaxation time constant associated to surface states; and (iii) the density of in-gap surface states, were all showing a well-marked maximum in the nearby value of the switch potential. This suggests that surface states are more influent in the nearby where photocurrent switch occurs.

1. Introduction

Bismuth vanadate ($BiVO_4$) is a suitable material for visible-light assisted oxygen evolution from water because of its n-type conductivity and appropriate band structure [1–3]. Up to now, its properties have been widely explored in various photoelectrode configurations [1–9]. However, some specific photoelectrochemical characteristics have not been reported yet. In particular, besides the expected anodic photocurrents observed on linear sweep voltammograms (LSV), small cathodic photocurrents are also measured at potentials less than 0.5 V (vs. RHE) [4,10]. Such behavior is not very common in semiconductor electrochemistry. It is known as photocurrent switching and a satisfactory explanation is available since 1980 [11]. Up to now, photocurrent switching has been observed not only on bulk semiconducting materials such as BiOI [12,13], but also on nano-sized photoelectrodes containing CdSe quantum dots [14]. It is worth mentioning here that the photocurrent switching phenomenon is different from the so-called "overshoot phenomenon". Photocurrent switching occurs when a n-type (p-type) semiconductor is illuminated and a cathodic (anodic) photocurrent is observed under reversed bias conditions [12–14]. The photocurrent overshoot [15] (also referred to as back electron/hole recombination [4]) occurs when the light is turned off, and the amount of photogenerated minority carriers (holes for n-type semiconductors) abruptly falls to zero and the current in the external circuit changes sign because majority carriers (electrons for n-type semiconductors) move to the surface to recombine with remaining minority carriers [15].

Regarding $BiVO_4$, to the best of our knowledge there is only one report by Kudo et al. in which photocurrent polarity switch is acknowledged: it has been attributed to hole doping due to potential scan [16]. Except this study, this specific phenomenon has received scarce attention from the scientific community. There are various experimental reports on $BiVO_4$ that show traces of photocurrent switching but this is usually not clearly put into evidence and analyzed. In several reports [5,17], measurements were made only at potentials above 0.5 V (vs. RHE), a potential range in which any eventual photocurrent switching cannot be put into evidence. In some cases [6], photocurrent spikes observed at potentials less than 0.5 V (vs. RHE) are not clear enough to assess the photocurrent switching phenomenon.

A literature survey on photocurrent switching shows that there is a general agreement to explain such phenomenon invoking the presence

* Corresponding author.
E-mail address: pierre.millet@u-psud.fr (P. Millet).

https://doi.org/10.1016/j.apcatb.2018.05.011
Received 1 April 2018; Received in revised form 1 May 2018; Accepted 4 May 2018
Available online 05 May 2018

of surface states [11–14,18]. A better understanding of the role of surface states during visible-light driven water splitting at the surface of photoelectrodes is a topic of great interest for the chemical community nowadays [19,20], because surface microscopic processes are usually a bottleneck in heterogeneous charge transfer [21].

In the literature, photoelectrochemical impedance spectroscopy (PEIS) has been commonly used to investigate the role of surface states during water splitting [21,22], and Gaussian-like distributions of the density of surface states have been obtained [22]. However, it is not always an easy task to assess the existence of surface states from PEIS measurements, mainly because simulated PEIS spectra are essentially the same, whether surface states are considered or not. PEIS can be used to assess the existence of surface states indirectly by fitting PEIS spectra [22], or by analyzing the potential dependence of derived kinetic parameters [23]. Alternatively, Intensity Modulated Photocurrent Spectroscopy (IMPS), whose theoretical foundations were derived by Peter et al. [24–27], is more appropriate than PEIS to observe experimentally surface states. The technique has already been successfully used to put into evidence their presence at the surface of TiO_2 photoanodes [28].

In this paper, new insights are provided on photo-electrocatalytic processes applied to environmental problems (water photo-dissociation) and on underlying basic phenomena such as photocurrent switching. More specifically, we report on photocurrent switching at $BiVO_4$ photoelectrodes and its analysis by IMPS. Whereas in the literature the existence and role of surface states in photo-electrochemistry has been mainly demonstrated indirectly (in most cases by fitting experimental impedance spectroscopy spectra with model equations that take into account the existence of such surface states [19–22,29]), we report here on direct experimental evidence. Experimental IMPS spectra reported here have very unusual features and, to the best of our knowledge, such features have been reported only two times before [30,31]. In addition to these experimental results, we also provide a new quantitative interpretation of these findings, definitively linked to photocurrent switching. The interest of these results is to uncover the impact of surface states in photoelectrochemical performance, but also to extend the range of applications of $BiVO_4$ photoelectrodes beyond visible-light harvesting for water oxidation. Indeed, n-type materials which provide photocathodic responses could be used for other environmentally-relevant reactions such as hydrogen evolution or carbon dioxide reduction. Photocurrent switching is also interesting for data-processing through the design of photoelectrochemical Boolean logical gates [32,33].

2. Theoretical background

When a semiconducting photoelectrode is illuminated with light radiations of energy greater than its band-gap, charge separation occurs and minority carriers (holes for a n-type semiconductor) drift and diffuse to the surface. The main driving force for charge separation comes from the band bending which takes place close to the surface over the space charge region, and this space charge layer is characterized by an associated capacitance (C_{SC}). The electric current associated to the flow of photogenerated charged species is represented here as I_0. At the interface between the semiconductor and an electrolytic solution, photogenerated minority carriers can be either transferred to the solution (the rate constant is k_t) or can recombine with majority carriers (e.g. electrons for a n-type semiconductor); in this case, the recombination rate constant is k_r. Non-ideal semiconductor – electrolyte interfaces are due to the presence of surface states, which can act as charge reservoirs and recombination centers, and can be characterized by an associated capacitance (C_{SS}). The situation is summarized in Fig. 1-a and -c, respectively.

Intensity Modulated Photocurrent Spectroscopy (IMPS) is a powerful technique that can be used to study the dynamics of charge transfer at the surface of illuminated photoelectrodes. IMPS principles have been described several times in the literature, with different degrees of detail [17,25,26,34]. Briefly, a constant electrical potential is imposed to the photoelectrode which is illuminated with a dc (constant) level of light. In addition, a small ac light perturbation is set and as a result, the photocurrent is periodic. In the absence of surface states (Fig. 1-a), the IMPS transfer function (H) is governed by Eq. (1). Conversely, when surface states are present but do not participate to the charge transfer process to the electrolyte (Fig. 1-c), the IMPS response follows Eq. (2) [26].

$$H = \frac{I_0[k_t + i\omega(C_{CELL}/C_{SC})]}{(k_t + k_r + i\omega)(1 + i\omega\tau)} \quad (1)$$

$$H = \frac{I_0[k_t + i\omega(C_{CELL}/C_{SC})]}{(k_t + k_r + i\omega)(1 + i\omega\tau) + \left(\frac{C_{SS}}{C_{SC} + C_H}\right)\left(\frac{i\omega}{1 + i\omega\tau_{SS}}\right)[1 + R_{SOL}C_H(k_t + i\omega)]} \quad (2)$$

In Eqs. (1) and (2), H is the IMPS transfer function, $\tau = R_{SOL}C_{CELL}$ where R_{SOL} is a resistance resulting from the electric wiring and the electrolyte layer (solution) between the surface and the reference tip, and C_{CELL} is the capacitance of the electrochemical cell (see Supporting information); τ_{SS} represents the relaxation time constant associated to surface states: $\tau_{SS} = R_{SS}C_{SS}$, where R_{SS} is the resistance associated to charge trapping by surface states (often referred to as R_{trap} [22,28]) and C_{SS} is the associated capacitance (also referred to as C_{trap} [22,28]) All other symbols have their usual meaning.

The Nyquist plot of Eq. (1) (the IMPS spectrum corresponding to the model in Fig. 1-a) is shown in Fig. 1-b. The complex plane is divided into four quadrants, counter-clockwise labeled I, II, III, IV, starting from the positive directions of both H' and H", as illustrated in Fig. 1-b and 1-d. According to Eq. (1), two semicircles develop in quadrants (I) and (IV). The high-frequency semicircle (in quadrant IV) corresponds to RC attenuation. The low-frequency semicircle (in quadrant I) is related to the rate constants of the system, as shown in Fig. 1-b.

Contrariwise, when there are surface states (and an associated surface state capacitance) that do not exchange charge with the solution (model of Fig. 1-c and Eq. (2)), the Nyquist representation of IMPS spectra may exhibit two semicircles in quadrant (I), the relative size of which is dependent on the rate constants and interfacial capacitances, as shown in Fig. 1-d. It is worth noting here that the graph of Eq. (2) (model of Fig. 1-c) can contain looped curves and other shapes, but the discussion of such situations lies outside the interest of the present article: the interested reader is referred to the original work by Ponomarev and Peter [26]. Furthermore, there is a third option of IMPS, covering the situation in which surface states do participate in the charge transfer process (equation 26 within reference [26]). In such a case, the absolute value of the modulated photocurrent may appear larger than I_0 (see Figure 9 within reference [26]), which is completely different to the behavior when surface states are present, but do not exchange charge with the electrolyte, which can be easily differentiated by visual inspection (compare, Figures 6 and 7 with Figure 9 in reference [26]).

Finally, it should be also noted that IMPS spectra reported in the literature are overwhelmingly plotted in Nyquist coordinates and that the model of Fig. 1-a and Eq. (1) is the most frequently used for analyzing experimental data [17,31,35,36]. Only few papers use the more elaborated model described in Fig. 1-c and Eq. (2) [28].

3. Experimental

3.1. $BiVO_4$ synthesis and photoelectrode preparation

In order to obtain the $BiVO_4$ photoelectrodes, $Bi(NO_3)_3{\cdot}5H_2O$ (Kanto Chemical, 99.9%) and NH_4VO_3 (Kanto Chemical, 99.9%) were dissolved in a HNO_3 solution (6.5 M) to make precursor solutions containing 100 mM of Bi and V. The precursor solution was then drop cast

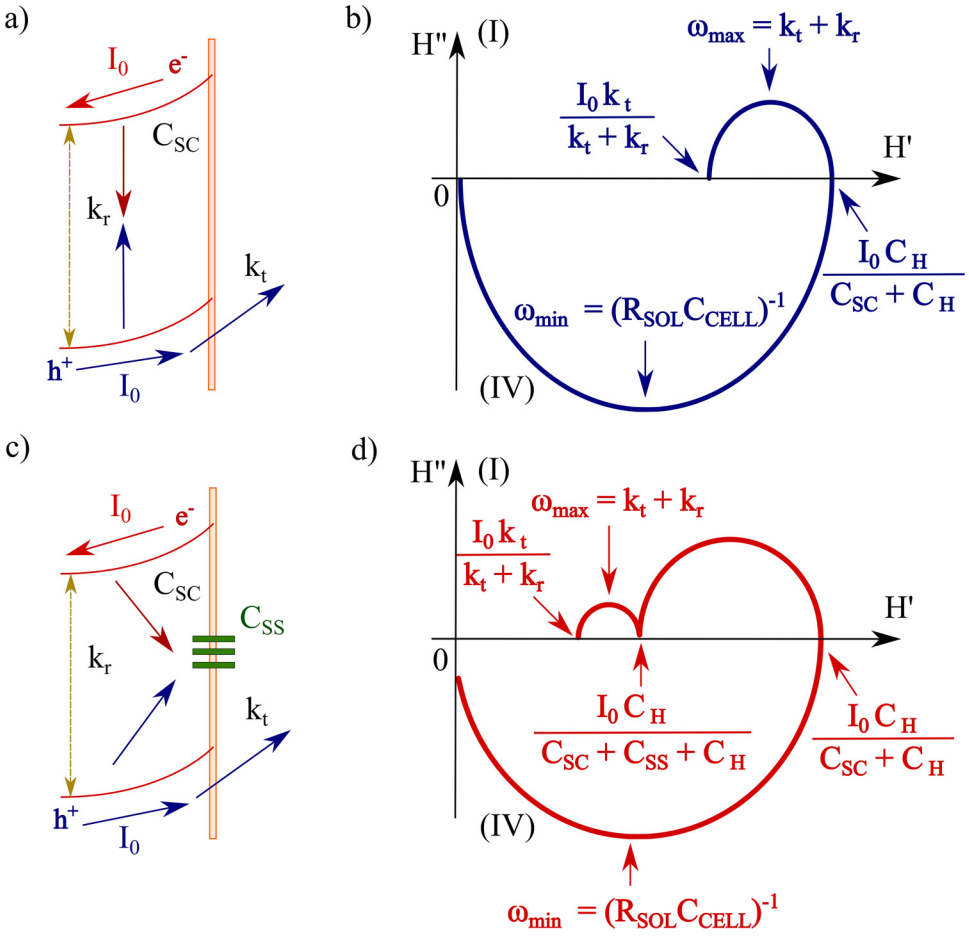

Fig. 1. Schematics of interfacial charge transfer and recombination kinetic models at illuminated semiconducting photoelectrodes; a) diagram of the simplest kinetic model where surface states are neglected; b) IMPS spectra of case 1-a in Nyquist coordinates with characteristic constant times; c) diagram of the kinetic model in the presence of surface states which here do not participate to charge transfer; d) IMPS spectra of case 1-c in Nyquist coordinates with characteristic constant times.

on top of a FTO substrate (TEC7, Aldrich) using a micropipette. Once the solution was dried with a heater from the FTO side, the substrate was calcined for 2 h in air at 773 K.

3.2. Electrochemistry

All electrochemical measurements were performed in aqueous Na_2SO_4 (0.1 M) using a three-electrode cell configuration. The FTO|$BiVO_4$ photoelectrode was used as the working electrode. Saturated calomel electrode (SCE) and a carbon plaque were employed as reference and counter electrodes, respectively. MilliQ water was used for all tests, and was obtained from a Merck Millipore device. All photoelectrochemical measurements were performed using a Modulab Solartron Analytical potentiostat, model 2100 A. The light source was controlled with a calibrated optical bench (Thorlabs Inc. DC2100), equipped with a calibrated LED. The intensity of light in mW/cm^2 was measured with a calibrated silicon detector coupled to the optical bench. The photoelectrochemical cell possessed a quartz window on the illumination side, and was provided by Pine Research Instrument Company. Intensity Modulated Photocurrent Spectroscopy (IMPS) spectra were recorded at different applied potentials and light intensities, as indicated in the text, over the 100 kHz–1 mHz frequency range. The small ac perturbation of light was set to 10% of the dc bias light. IMPS data were fitted in Matlab R2014b with a homemade code.

4. Results and discussion

4.1. Photocurrent characteristics of $BiVO_4$ photoelectrodes

First, polarization curves of $BiVO_4$ photoelectrodes were recorded under chopped illumination conditions over a potential window (from −0.1 up to +1.3 V/SCE) larger than those reported in several previous studies [1,6,17]. Fig. 2-a shows a typical cyclic voltammogram (CV) measured in 0.1 M Na_2SO_4. The curve in blue is the usual photoanodic response of a n-type semiconductor. The curve in red shows the unusual cathodic photocurrent, which demonstrates that this $BiVO_4$ photoelectrode exhibits the photocurrent switching phenomenon discussed in the introduction section.

There are two main interesting features in this CV that are worth to be discussed in detail. First, the potential at which there is a change in the sign of the photocurrent is not unique, and depends on whether the scan is performed in the anodic or the cathodic direction. Fig. 2-b shows three consecutive CVs under the same operating conditions of Fig. 2-a (note that in Fig. 2-b the current density is plotted as a function of time). The applied potential is plotted in green. With such a representation it becomes clear that during the forward scan, the sign of the photocurrent changes from negative to positive at +0.16 V (vs. SCE), and during the backward scan the current switches from positive to negative at +0.63 V (vs. SCE). The hysteresis has a somewhat large magnitude of 470 mV.

The photocurrent switching phenomenon can be schematically interpreted with the aid of Fig. 2-c where the energy (upwards) and potential (downwards) scales are represented on the left-hand side of the plot. In the semiconductor (left side of the interface), anodic photocurrents can flow across the interface when the potential of the edge of the valence band is more positive than the potential of the hole acceptor in solution (thick horizontal black line on the right side of the interface). However, when an external negative potential bias is applied (cathodic polarization), the bands can move upwards and eventually an electrode potential is attained where the edge of the valence band is more negative than the potential of the hole acceptor in solution. Such model (shown in Fig. 2-c) is not frequently used in

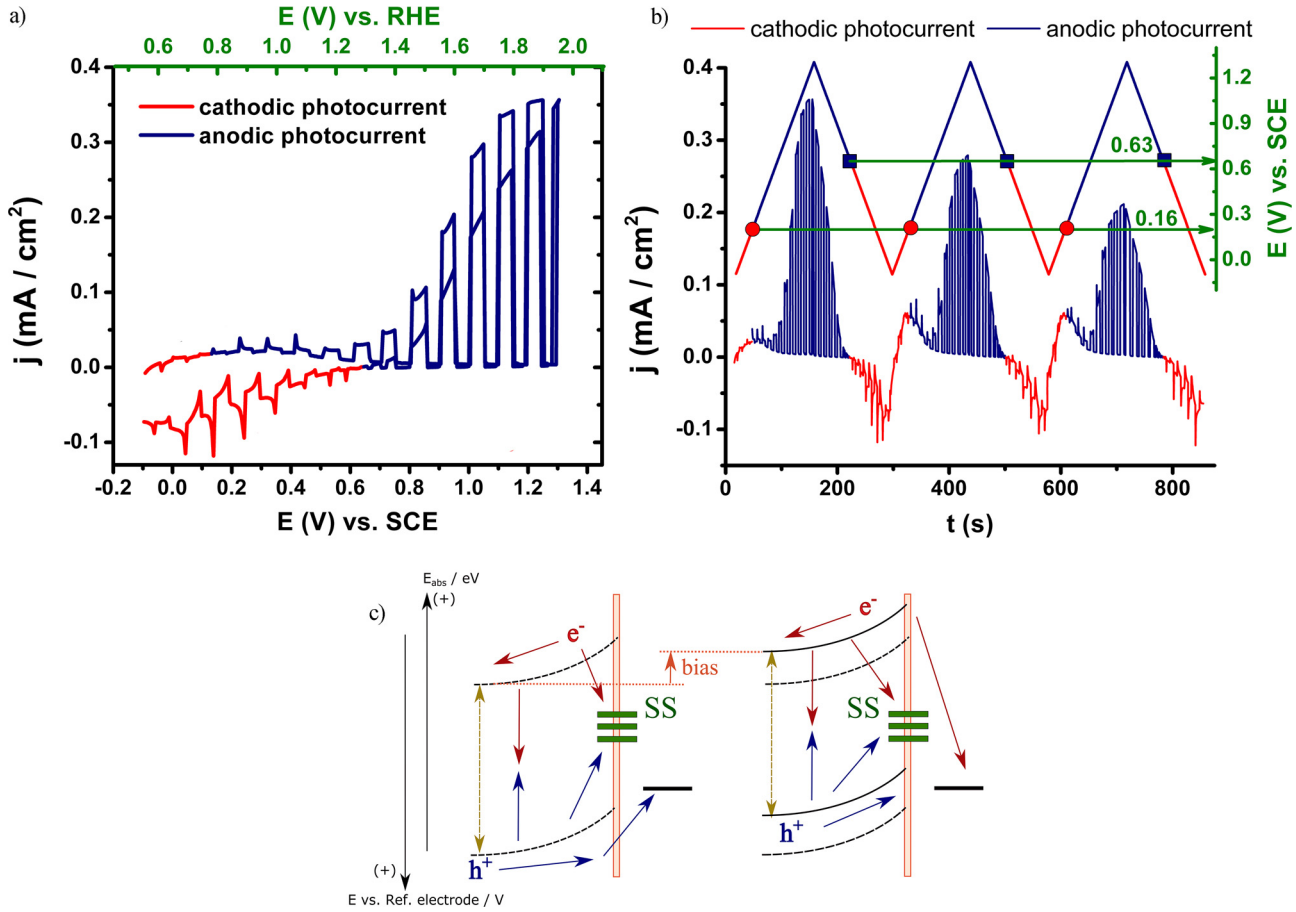

Fig. 2. a) Cyclic voltammogram of a $BiVO_4$ photoelectrode under chopped illumination; cathodic photocurrents are shown in red, and anodic photocurrents in blue; b) Three consecutive cyclic voltammograms under chopped illumination. Again, cathodic photocurrents are shown in red, and anodic photocurrents in blue. The abscissa corresponds to the time; the left ordinate axis corresponds to the observed current density while the right ordinate axis represents the applied potential (the potential window is identical to the one of Fig. 2-a); c) scheme representing an explanation for the photocurrent switching phenomenon (For interpretation of the references to color in this figure legend, the reader is referred to the web version of this article).

photoelectrochemistry: most models of the semiconductor|electrolyte interface are based on the idea of band-edge pinning at the interface. However, band-edges may move with bias, as explained elsewhere (see for example reference [37]); moreover, despite its limitations, the model of Fig. 2-c is currently the most appropriate to analyze photocurrent switch [12,18].

When the potential of the edge of the valence band becomes more negative than the potential of the hole acceptor in solution, hole transfer to the electrolyte is no longer thermodynamically possible (Fig. 2-c, right). If surface states of adequate energy are present (as depicted on the right side of Fig. 2-c) electron transfer could occur towards the solution either through surface states [18] or through the conduction band [12], and a cathodic photocurrent is consequently observed. In this work, the electrochemical cell was carefully de-aerated and the measurements were performed under Ar atmosphere. Therefore, anodic photocurrents are due to water oxidation into oxygen and cathodic photocurrents are due to water reduction in hydrogen. Of course, the process of charging – discharging the surface states tends to reconfigure the potential distribution at the interface, and when a potentiodynamic scan of the photoelectrode is carried out (as this is the case during a CV), the static scheme of Fig. 2-c is too simplistic to explain why there are two different switch potentials depending on the direction of the scan. This fact certainly has its origin in the dynamic reconfiguration of interfacial potential drop brought about by the dynamic charge – discharge of surface states.

A second feature of interest observed on the experimental CVs shown in Fig. 2-a and -b is that the photocurrent spikes are much more marked in the cathodic photocurrent region than in the anodic photocurrent region. This is an indication that electron/hole recombination is faster in cathodic potential regions [15].

4.2. *Intensity modulated photocurrent spectroscopy response of $BiVO_4$ photoelectrodes*

Some of the characteristics of the $BiVO_4$ photoelectrodes reported in the previous section are novel and interesting. In order to better understand the factors governing the observed photoelectrochemistry and to perform a quantitative kinetic analysis, IMPS was selected as the most appropriate experimental technique. IMPS spectra have been recorded in both the photoanodic and photocathodic potential regions.

Fig. 3-a shows typical Nyquist plots of IMPS spectra measured at constant potential (+1.2 V vs. SCE) but using different light intensities. In order to show the existence of two semicircles in quadrant (I) of the complex plane, the IMPS spectrum measured at 529.03 mW/cm^2 has been plotted separately (inset of Fig. 3-a) using non-orthonormal axes. IMPS semicircles appear flattened (i.e., their center is not located on the real axis of the plots), a feature due to non-ideality and which is usually attributed to surface heterogeneity [15,38] The shape of these experimental IMPS spectra is consistent with the model responses of Fig. 2-b, and therefore excludes both the possibility to ignore the effect of surface states (model response of Fig. 1-b) and the possible interpretation of surface states participation in charge transfer [26].

In quadrant (I), there are two semicircles (Fig. 3-a and inset). This is in agreement with Eq. (2), and an indication that the simplest model of

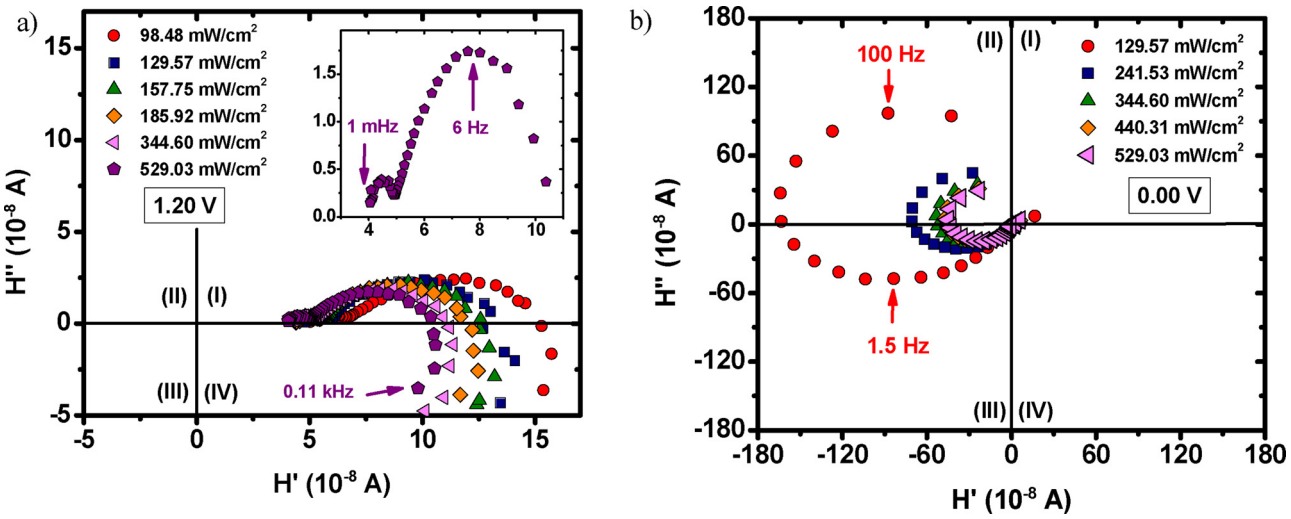

Fig. 3. Nyquist plots of typical IMPS spectra measured on $BiVO_4$ photoelectrodes; a) data obtained in the anodic photocurrent region at +1.20 V vs. SCE using different illumination intensities; b) data obtained in the cathodic (switched) photocurrent region at 0.00 V vs. SCE under different illumination intensities. Fitted curves are provided as supporting information.

Eq. (1) does not apply here. The high frequency semicircle is due to the time constant of the cell (see details in Fig. S1-d). The observation of Fig. 3-a confirms the presence of surface states which do not exchange charge with the electrolyte. The semicircles that develop in the low frequency range (quadrant I) are found between $2.65{\cdot}10^{-3}$ and $1{\cdot}10^{-3}$ Hz. Therefore, the charge transfer and recombination rate constants are very small.

Back to the main discussion of our results, when the electrode potential is made more negative, the IMPS spectra continually shrink until the IMPS no longer develops in quadrants (I) and (IV) of the complex plane, but develops in quadrants (II) and (III) instead (see Figs. 3-b and S2). The sliding of the IMPS spectra to the other side of the complex plane occurs at the electrode potential for which there is a change in the sign of the photocurrent (from anodic to cathodic and vice versa). Therefore, the sliding from quadrants (I-IV) to quadrants (II-III) is linked to the sign of the photocurrent only. It should be noted that IMPS analysis was performed potentiostatically. The sliding of IMPS spectra was observed at the switch potential corresponding to the backwards scan of the CV of Fig. 2-a and 3-b, in contrast to the potentiodynamic CV where two switch potentials were reported.

To the best of our knowledge, a satisfactory explanation of the shape of IMPS spectra developing in quadrant (II) and (III) has not been provided yet. According to the CV of Figs. 2-a and 3-b, there is a change in the sign of the photocurrent at potentials lower than +0.63 V (vs. SCE). The sign of the IMPS transfer function (represented here as H) also changes. Considering that H is a complex function, when there is a change in the sign of the photocurrent sign, the sign of both the real and imaginary part of H changes. This is equivalent to a 180° rotation around the origin of the complex plane. Consequently, the high-frequency attenuation semicircle is shifted to quadrant (II), and the kinetically-relevant low-frequency semicircle is shifted to quadrant (III). This is what is observed experimentally (Figs. 3-b and S3–S5) and is in agreement to previous experimental observations of IMPS developing in quadrants (II–III) [30,31]. Despite this change, IMPS spectra measured in both potential range exhibit similar features. Therefore, experimental IMPS spectra recorded in both potential ranges can be fitted using the same model.

Keeping in mind that in Fig. 3-b the kinetic semicircle develops in the (III) quadrant, it can be inferred that recombination is much faster than charge transfer because the low-frequency limit of IMPS tends towards the coordinate origin, as opposed to Fig. 3-a, where the low frequency limit of IMPS tends to the real axis (abscissa) but significantly separated from the coordinate origin. This qualitative interpretation is in agreement with the photocurrent spikes observed in the cathodic region, and the absence of spikes in the anodic photocurrent region (Fig. 3-a and -b).

4.3. Photoelectrochemical rate constants and capacitances derived for $BiVO_4$ photoelectrodes

Quantitative values of microscopic parameters (rate constants and capacitances) have been obtained by fitting experimental IMPS spectra with model Eq. (2). The charge transfer and recombination rate constants obtained at different potentials are plotted in Fig. 4-a. Overall, it was found that the charge transfer rate constant is almost independent of light power and electrode potential. The rate constant for charge transfer was found equal to $(4.3 \pm 0.5){\cdot}10^{-2}\,s^{-1}$. The independence of k_t versus applied potential is not unusual in photoelectrochemistry [39], and is due to the small potential drop across the Helmholtz layer as compared to the space charge. On the contrary, it was found that there is a variation of the recombination rate constant k_r versus the applied electrode potential. In the potential region where anodic photocurrents are measured, k_r is small and close to k_t, i.e., $k_r = (7.40 \pm 0.06){\cdot}10^{-2}\,s^{-1}$. In the potential region where cathodic photocurrents are measured, the recombination rate constant increases notably by two orders of magnitude to reach a value of $7 \pm 2\,s^{-1}$. Such difference indicates an important change in the characteristics of the interface as the potential is scanned from the anodic to the cathodic photocurrent region.

The space charge capacitance (C_{SC}) and Helmholtz capacitance (C_H) were also determined from the fits. All the capacitances that were measured on the $BiVO_4$ photoelectrodes were found to have a rather similar value, within the range reported for other photoelectrodes [22]. Neither C_{SC} nor C_H presented a clear trend with any of the experimental parameters (Fig. 4-b). In particular C_{SC} did not follow the Mott-Schottky relation [40], and this is attributed to the manifest presence of trapping surface states. The Bode representation of IMPS spectra (Fig. S1-d) shows that the minimum in the RC attenuation (which appears in quadrant (IV) of the complex-plane) occurs at the same frequency, regardless the applied potential.

Concerning the surface states, there are two main physical parameters that dictate their influence on the photoelectrode: their surface state resistance (R_{SS}) and their surface state capacitance (C_{SS}). As can be seen from Fig. 4-b, R_{SS} remains essentially constant ($R_{SS} = 600 \pm 2\,\Omega\,cm^2$). This is an indication that, for the system under consideration, surface states do not participate to the charge transfer

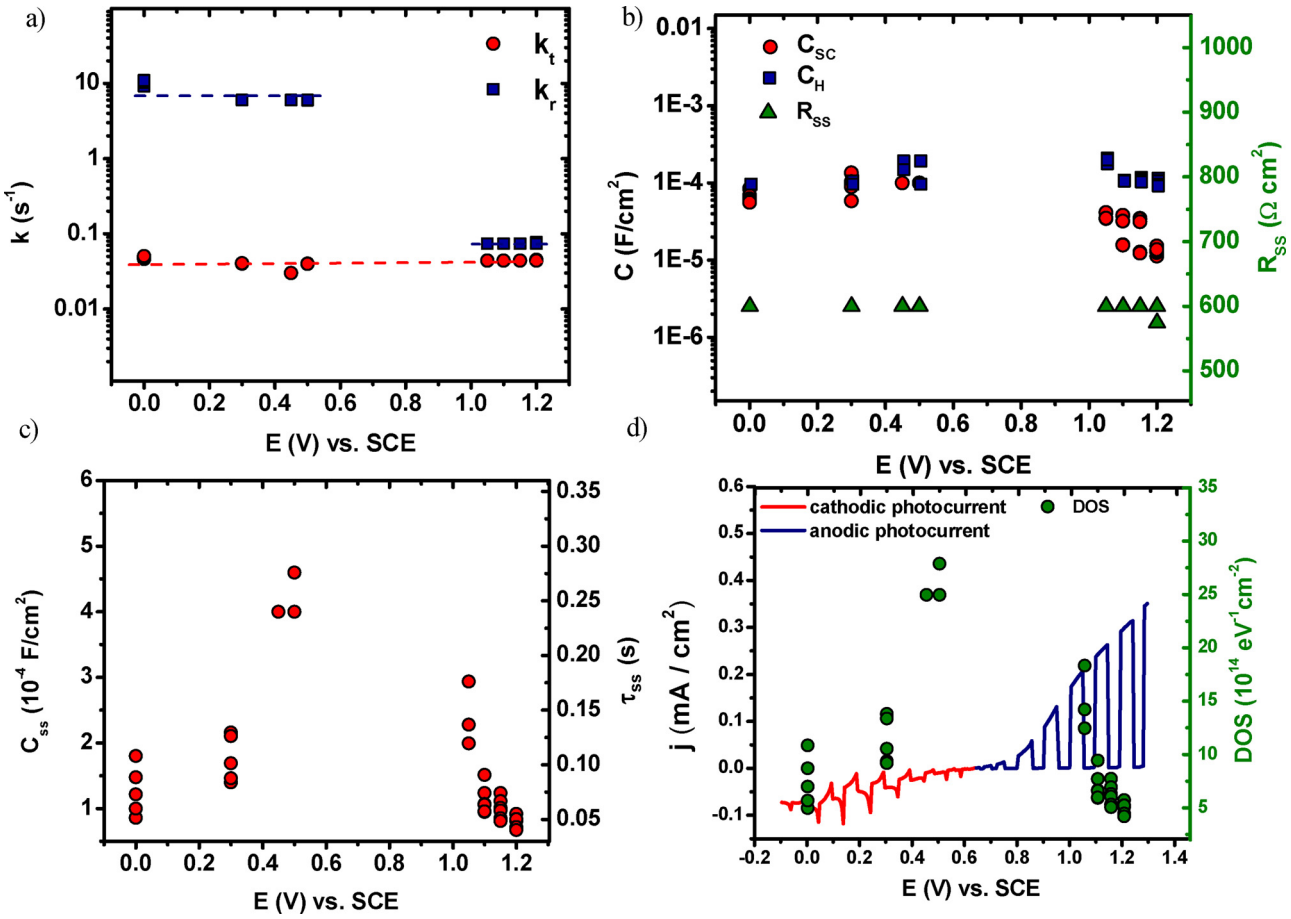

Fig. 4. a) Kinetic constants for the $BiVO_4$ material as a function of electrode potential. Dashed lines have been put as a guide to the eye; b) space charge capacitance, Helmholtz capacitance and surface states resistance as a function of electrode potential; c) surface states capacitance and relaxation time associated to surface states as a function of electrode potential; d) DOS of in-gap surface states superimposed to the backwards scan of the cyclic voltammogram under chopped illumination.

process. It can also be shown that the behavior of surface states capacitance is governed by Eq. (3) [22,41]

$$C_{SS} = AqN_{SS}\frac{\partial f_{ss}}{\partial E_F} \tag{3}$$

where A is the area of the electrode, q represents the elemental charge, N_{SS} is the density of surface states, f_{ss} stands for the fractional occupancy of the state and E_F is the Fermi level of the states.

According to Eq. (3), C_{SS} possesses a maximum when the electrode potential matches the energy of the surface state, and thus a Gaussian-like distribution of the surface state capacitance is to be expected [20–22,29,41]. In this case, a plot of the surface states capacitance vs. the electrode potential shows such a Gaussian-like shape (Fig. 4-c). Likewise, the time constant related to surface states' charging passes through a maximum in the nearby of the electrode potential where photocurrent changes its sign (Fig. 4-c). Knowing the value of the surface state capacitance, it is also possible to calculate the density of states, $g(E_{Fn})$ or DOS, of in-band surface states according to Eq. (4) [22,42]

$$C_{SS}(E) = qg(E_{Fn}) \tag{4}$$

The calculated DOS for $BiVO_4$ photoelectrodes (Fig. 4-d) agrees quantitatively with previous work on hematite photoelectrodes [22], and is one order of magnitude higher than the values reported for n-GaAs(100) and p-GaAs(100) [29]. Fig. 4-d also shows the polarization curve during the backwards scan for comparison. It may be appreciated that the effect of surface states is notable over the whole potential range studied here. Interestingly, (i) the surface states capacitance, (ii) the relaxation time associated to surface states and (iii) the density of in-gap states, all pass through a maximum very close to the electrode potential for which there is a change in photocurrent sign.

The comparison of this results with other previously published is eloquent. Indeed, so far the effect of surface states has been reported for systems where no photocurrent switch existed [19,20,22]. In such cases, the maximum of the surface states capacitance and therefore the maximum density of in-gap states was found in the nearby of the photocurrent onset. In our case, the maximum of the in-gap states was found to be in the nearby of the switching potential, clearly suggesting that the influence of surface states is more pronounced where the photocurrent changes its sign.

5. Conclusions

$BiVO_4$ photoelectrodes have been prepared and their activity towards water oxidation and reduction have been analyzed. The photoelectrodes have first been characterized by cyclic voltammetry under chopped illumination conditions. During anodic potential scans, positive (anodic) photocurrents have been recorded at potentials higher than +0.16 V (vs. SCE); negative (cathodic) photocurrents have also been recorded during the cathodic scans for potentials below +0.63 V (vs. SCE). In order to better understand the origin of underlying microscopic phenomena, a thorough investigation of the photoelectrodes has been performed using Intensity Modulated Photocurrent Spectroscopy (IMPS), under visible-light irradiation. In the potential region of anodic photocurrent, complex-plane representations of IMPS spectra show two semicircles in quadrant (I), a feature which is

characteristic of semiconductors with high surface states capacitance. Conversely, in the potential region of cathodic photocurrent, complex-plane representations of IMPS spectra show two semicircles in quadrants (II) and (III). These results were interpreted as a rotation of the Nyquist representation of IMPS around the coordinate origin, as a consequence of the sign change of the photocurrent. Microscopic parameters have been determined by fitting experimental IMPS spectra with a model that takes into account the existence of surface states. Overall, the charge transfer rate constant was found to be small ($4.3 \pm 0.5{\cdot}10^{-2}\,s^{-1}$) over the whole potential range of investigation. Such low value was attributed to the small potential drop across the Helmholtz layer. The recombination rate constant ($7.40 \pm 0.06{\cdot}10^{-2}\,s^{-1}$ in the anodic photocurrent region, and $7 \pm 2\,s^{-1}$ in the cathodic photocurrent region), showed that important changes occur at the interface when the photocurrent switches. Helmholtz and space charge capacitances did not present any characteristic trends with electrode potential and this was attributed to the manifested presence of surface states with high capacitance. The resistance of surface states deduced from the fits was found potential independent (a constant value of $600 \pm 2\,\Omega\,cm^2$ was obtained). This is an indication that surface states can trap charge carriers but do not participate to the charge transfer process towards the electrolyte. Such traps accumulate charge and act as recombination centers only. Another interesting finding of this work was the evolution of the surface state capacitance as a function of the electrode potential. A Gaussian-like shape was observed as predicted by theory. Interestingly, (i) the surface states capacitance, (ii) the relaxation time associated to surface states and (iii) the DOS in-gap surface states, all show a well-marked maximum in the nearby of the potential where photocurrent changed its sign. For systems showing photocurrent switching, the role of surface states appears to be more pronounced at the switching potential.

Acknowledgements

Manuel Antuch is thankful for a French Ministerial Scholarship and the Initiative d'Excellence (IDEX) program as a Ph.D. student. The authors gratefully acknowledge Diana Dragoe for the acquisition of XPS spectra and François Brisset for SEM images.

Appendix A. Supplementary data

Supplementary material related to this article can be found, in the online version, at doi:https://doi.org/10.1016/j.apcatb.2018.05.011.

References

[1] Y. Ma, S.R. Pendlebury, A. Reynal, F. Le Formal, J.R. Durrant, Dynamics of photogenerated holes in undoped BiVO4 photoanodes for solar water oxidation, Chem. Sci. 5 (2014) 2964–2973, http://dx.doi.org/10.1039/c4sc00469h.
[2] Y. Liang, J. Messinger, Improving BiVO4 photoanodes for solar water splitting through surface passivation, Phys. Chem. Chem. Phys. 16 (2014) 12014–12020, http://dx.doi.org/10.1039/c4cp00674g.
[3] B. Xiao, L. Lin, J. Hong, H. Lin, Y. Song, Synthesis of a monoclinic BiVO4 nanorod array as the photocatalyst for efficient photoelectrochemical water oxidation, RSC Adv. 7 (2017) 7547–7554, http://dx.doi.org/10.1039/C6RA28262H.
[4] Y. Ma, F. Le Formal, A. Kafizas, S.R. Pendlebury, J.R. Durrant, Efficient suppression of back electron/hole recombination in cobalt phosphate surface- modified undoped bismuth vanadate photoanodes, J. Mater. Chem. A 3 (2015) 20649–20657, http://dx.doi.org/10.1039/C5TA05826K.
[5] L. Zhang, E. Reisner, J.J. Baumberg, Environmental science Al-doped ZnO inverse opal networks as e ffi cient electron collectors in BiVO4 photoanodes for solar water oxidation, Energy Environ. Sci. 7 (2014) 1402–1408, http://dx.doi.org/10.1039/c3ee44031a.
[6] S. Hernández, G. Gerardi, K. Bejtka, A. Fina, N. Russo, Environmental evaluation of the charge transfer kinetics of spin-coated BiVO4 thin films for sun-driven water photoelectrolysis, Appl. Catal. B Environ. 190 (2016) 66–74, http://dx.doi.org/10.1016/j.apcatb.2016.02.059.
[7] L. Yun, Z. Yang, Z.-B. Yu, T. Cai, Y. Li, C. Guo, C. Qia, T. Ren, Synthesis of four-angle star-like CoAl-MMO/BiVO4 p–n heterojunction and its application in photocatalytic desulfurization, RSC Adv. 7 (2017) 25455–25460, http://dx.doi.org/10.1039/C7RA03012F.
[8] B.J. Trzesniewski, W.A. Smith, Photocharged BiVO4 photoanodes for improved solar water splitting, J. Mater. Chem. A 4 (2016) 2919–2926, http://dx.doi.org/10.1039/C5TA04716A.
[9] Z. Zhang, M. Wang, W. Cui, H. Sui, Synthesis and characterization of a core–shell BiVO4@g-C3N4 photo-catalyst with enhanced photocatalytic activity under visible light irradiation, RSC Adv. 7 (2017) 8167–8177, http://dx.doi.org/10.1039/C6RA27766G.
[10] H.S. Park, H. Ha, R.S. Ruoff, A.J. Bard, On the improvement of photoelectrochemical performance and finite element analysis of reduced graphene oxide – BiVO 4 composite electrodes, J. Electroanal. Chem. 716 (2014) 8–15, http://dx.doi.org/10.1016/j.jelechem.2013.08.036.
[11] H.R. Sprünken, R. Schumacher, R.N. Schindler, Photoreduction processes on n-TiO2 electrodes, Ber. Bunsenges. Phys. Chem. 84 (1980) 1040–1045.
[12] P. Kwolek, K. Szaciłowski, Photoelectrochemistry of n-type bismuth oxyiodide, Electrochim. Acta 104 (2013) 448–453, http://dx.doi.org/10.1016/j.electacta.2012.10.001.
[13] M.E. Kazyrevich, M.V. Malashchonak, A.V. Mazanik, E.A. Streltsov, A.I. Kulak, C. Bhattacharya, Photocurrent switching effect on platelet-like BiOI electrodes: influence of redox system, light wavelength and thermal treatment, Electrochim. Acta 190 (2016) 612–619, http://dx.doi.org/10.1016/j.electacta.2015.12.229.
[14] M. El Harakeh, L. Alawieh, S. Saouma, L.I. Halaoui, Charge separation and photocurrent polarity-switching at CdS quantum dots assembly in polyelectrolyte interfaced with hole scavengers, Phys. Chem. Chem. Phys. 11 (2009) 5962–5973, http://dx.doi.org/10.1039/b820895f.
[15] H.-J. Lewerenz, L. Peter, Photoelectrochemical Water Splitting Materials, Processes and Architectures, RSC Publishing, 2013.
[16] A. Iwase, A. Kudo, Photoelectrochemical water splitting using visible-light-responsive BiVO4 fine particles prepared in an aqueous acetic acid solution, J. Mater. Chem. 20 (2010) 7536–7542, http://dx.doi.org/10.1039/c0jm00961j.
[17] C. Zachäus, F.F. Abdi, L.M. Peter, R. van de Krol, Photocurrent of BiVO4 is limited by surface recombination, not surface catalysis, Chem. Sci. 8 (2017) 3712–3719, http://dx.doi.org/10.1039/C7SC00363C.
[18] A. Podborska, B. Gawel, L. Pietrzak, I.B. Szymańska, J.K. Jeszka, W. Łasocha, K. Szacilowski, Anomalous photocathodic behavior of CdS within the urbach tail region, J. Phys. Chem. C 113 (2009) 6774–6784, http://dx.doi.org/10.1021/jp809794s.
[19] K.J. Pyper, J.E. Yourey, B.M. Bartlett, Reactivity of CuWO4 in photoelectrochemical water oxidation is dictated by a midgap electronic state, J. Phys. Chem. C 117 (2013) 24726–24732, http://dx.doi.org/10.1021/jp408434v.
[20] Y. Gao, T.W. Hamann, Elucidation of CuWO4 surface States during photoelectrochemical Water oxidation, J. Phys. Chem. Lett. 8 (2017) 2700–2704, http://dx.doi.org/10.1021/acs.jpclett.7b00664.
[21] B. Klahr, T. Hamann, Water oxidation on hematite photoelectrodes: insight into the nature of surface states through in situ spectroelectrochemistry, J. Phys. Chem. C 118 (2014) 10393–10399, http://dx.doi.org/10.1021/jp500543z.
[22] B. Klahr, S. Gimenez, F. Fabregat-Santiago, T. Hamann, J. Bisquert, Water oxidation at hematite photoelectrodes: the role of surface states, J. Am. Chem. Soc. 134 (2012) 4294–4302, http://dx.doi.org/10.1021/ja210755h.
[23] K.G. Upul Wijayantha, S. Saremi-Yarahmadi, L.M. Peter, Kinetics of oxygen evolution at α-Fe2O3 photoanodes: a study by photoelectrochemical impedance spectroscopy, Phys. Chem. Chem. Phys. 13 (2011) 5264, http://dx.doi.org/10.1039/c0cp02408b.
[24] Ea. Ponomarev, L.M. Peter, A comparison of intensity modulated photocurrent spectroscopy and photoelectrochemical impedance spectroscopy in a study of photoelectrochemical hydrogen evolution at p-InP, J. Electroanal. Chem. 397 (1995) 45–52, http://dx.doi.org/10.1016/0022-0728(95)04148-9.
[25] L.M. Peter, E.A. Ponomarev, D.J. Fermín, Intensity-modulated photocurrent spectroscopy: reconciliation of phenomenological analysis with multistep electron transfer mechanisms, J. Electroanal. Chem. 427 (1997) 79–96, http://dx.doi.org/10.1016/S0022-0728(96)05033-4.
[26] Ea. Ponomarev, L.M. Peter, A generalized theory of intensity modulated photocurrent spectroscopy (IMPS), J. Electroanal. Chem. 396 (1995) 219–226, http://dx.doi.org/10.1016/0022-0728(95)04115-5.
[27] R. Peat, L.M. Peter, Characterization of semiconductor electrodes by intensity modulated spectroscopy (IMPS), J. Electrochem. Soc. 133 (1986) C334.
[28] H. Cachet, E.M.M. Sutter, Kinetics of Water oxidation at TiO2 nanotube arrays at different pH domains investigated by electrochemical and light-modulated impedance spectroscopy, J. Phys. Chem. C 119 (2015) 25548–25558, http://dx.doi.org/10.1021/acs.jpcc.5b06103.
[29] M. Enache, C. Negrila, M. Anastasescu, G. Dobrescu, M.F. Lazarescu, V. Lazarescu, Surface states- and field-effects at GaAs (100) electrodes in sodium dodecyl sulfate acid solution, J. Electrochem. Soc. 165 (2018) 3008–3017, http://dx.doi.org/10.1149/2.0031804jes.
[30] J.F. Miethe, F. Lübkemann, J. Poppe, F. Steinbach, D. Dorfs, N.C. Bigall, Spectroelectrochemical investigation of the charge carrier kinetics of gold-decorated cadmium chalcogenide nanorods, ChemElectroChem 5 (2017) 175–186, http://dx.doi.org/10.1002/celc.201700798.
[31] T. Oekermann, D. Schlettwein, N.I. Jaeger, Charge transfer and recombination kinetics at electrodes of molecular semiconductors investigated by intensity modulated photocurrent spectroscopy, J. Phys. Chem. B 105 (2001) 9524–9532.
[32] G. Loget, G. Li, B. Fabre, Logic gates operated by bipolar photoelectrochemical wated splitting, Chem. Comm. 51 (2015) 11115–11118.
[33] K. Szacilowski, W. Macyk, G. Stochel, Light-Driven OR and XOR programmable chemical logic gates, J. Am. Chem. Soc. 128 (2006) 4550–4551.
[34] C.Y. Cummings, F. Marken, L.M. Peter, A. a Tahir, K.G.U. Wijayantha, Kinetics and mechanism of light-driven oxygen evolution at thin film α-Fe2O3 electrodes, Chem.

Commun. 48 (2012) 2027–2029, http://dx.doi.org/10.1039/c2cc16382a.
[35] A.Y. Ahmed, T. Oekermann, P. Lindner, D. Bahnemann, Comparison of the photoelectrochemical oxidation of methanol on rutile TiO2 (001) and (100) single crystal faces studied by intensity modulated photocurrent spectroscopy, Phys. Chem. Chem. Phys. 14 (2012) 2774–2783, http://dx.doi.org/10.1039/c2cp23416e.
[36] H.K. Dunn, J.M. Feckl, A. Müller, D. Fattakhova-Rohlfing, S.G. Morehead, J. Roos, L.M. Peter, C. Scheu, T. Bein, Tin doping speeds up hole transfer during light-driven water oxidation at hematite photoanodes, Phys. Chem. Chem. Phys. 16 (2014) 24610–24620, http://dx.doi.org/10.1039/C4CP03946G.
[37] J.E. Thorne, S. Li, C. Du, G. Qin, D. Wang, Energetics at the surface of photoelectrodes and its influence on the photoelectrochemical properties, J. Phys. Chem. Lett. 6 (2015) 4083–4088, http://dx.doi.org/10.1021/acs.jpclett.5b01372.
[38] R. Peat, L.M. Peter, Intensity modulated photocurrent spectroscoy of n-GaAs, Ber. Bunsenges. Phys. Chem. 91 (1987) 381–386.
[39] M.J. Cass, N.W. Duffy, L.M. Peter, S.R. Pennock, S. Ushiroda, A.B. Walker, Microwave reflectance studies of photoelectrochemical kinetics at semiconductor electrodes. 1. Steady-State, transient, and periodic responses, J. Phys. Chem. B 107 (2003) 5857–5863, http://dx.doi.org/10.1021/jp030088d.
[40] K. Gelderman, L. Lee, S.W. Donne, Flat-band potential of a semiconductor: using the Mott–Schottky equation, J. Chem. Educ. 84 (2007) 685–688.
[41] R. Memming, Semiconductor Electrochemistry, 2nd ed., Wiley-VCH Verlag GmbH and Co. KGaA, 2015.
[42] F. Fabregat-santiago, G. Garcia-Belmonte, I. Mora-Sero, J. Bisquert, Characterization of nanostructured hybrid and organic solar cells by impedance spectroscopy, Phys. Chem. Chem. Phys. 13 (2011) 9083–9118, http://dx.doi.org/10.1039/c0cp02249g.